JOURNAL OF PROPULSION AND POWER
Vol. 23, No. 6, November–December 2007

# Effect of Aluminum on Heat Flux from a Simulated Rocket Propellant Flame

R. B. White,* S. W. Dean,* and M. L. Pantoya*
*Texas Tech University, Lubbock, Texas 79409*
D. A. Hirschfeld†
*New Mexico Institute of Mining and Technology, Socorro, New Mexico 87801*
and
W. Gill‡ and W. W. Erikson‡
*Sandia National Laboratories, Albuquerque, New Mexico 87185*

DOI: 10.2514/1.28161

**Aluminum particles have been shown to enhance the performance in propellant systems by reacting and releasing significant chemical energy that contributes to the overall heat release. However, the heat transfer characteristics from a propellant to a target are not well understood. In this study, impinging flow geometries of a simulated propellant flame seeded with aluminum particles were investigated. Although the contribution of aluminum was the main focus of this study, inert powders of alumina-titania and yttria stabilized zirconia were also used to compare and quantify the heat flux contributions of reacting, melting, and nonmelting powders, respectively. An oxygen–acetylene torch seeded with aluminum, alumina-titania, or yttria stabilized zirconia was used to analyze the different heat transfer characteristics from each material. Copper coupons captured and quenched reacting particulates from the flame. A scanning electron microscope with energy dispersive spectroscopy and a differential scanning calorimeter were used to examine the degree of completion of aluminum oxidation. Results show that yttria stabilized zirconia experience a 1.9% increase in heat flux compared with gas-only flames. Flames seeded with alumina-titania showed an 80.2% increase in heat flux, whereas aluminum particles provide a 232.7% gain over gas-only flames. Results from the differential scanning calorimeter show that aluminum consumption percentages for flames with a 2.5 oxygen–fuel ratio are an average of 8.6% higher than those for a 1.5% oxygen–fuel ratio. The percent of aluminum consumed in the reaction generally increases with standoff distance.**

## Introduction

ALONG with the increased performance from the addition of aluminum (Al) to solid rocket propellant comes an increased potential for hazardous scenarios. Understanding the fire environment presented by aluminum seeded propellant flames is integral to the development of vehicle subsystems which respond in a safe and predictable manner during accident situations in which the propellant is burning in an off-design situation with circumstances much different than those of traditional solid propellant combustion. Understanding the role of the aluminum particles in the combustion and heat transfer associated with accident fire plumes is necessary for describing the thermal environment.

Fundamental studies involving the combustion of aluminum particles have been performed by numerous researchers and review papers are available [1–12]. This work focuses on the addition of Al particles to solid propellants that ultimately causes an increase in propellant burn rate. Davis [13] examined burn rates of ammonium perchlorate (AP) and paraformaldehyde propellants. The formulations contained <1% Al by mass. This study examined the effect of Al particle size on burn rate and used Al particles ranging from 53 to 103 $\mu$m in diameter. The results did not precisely follow the $D^2$ law; instead, an exponent of 1.8 was found to fit the experimental data well. Melcher et al. [14] used an AP/hydroxyl-terminated polybutadiene (HTPB) propellant and 106 $\mu$m Al particles to demonstrate the diameter dependence on burn time and showed similar results. Other fundamental studies showed that Al reacts as alumina accumulates in an "oxide cap" created on the molten Al surface as the elemental Al gasifies and reacts [15]. Though important to understanding propellant behavior, burn rate is only one property desired from propellant studies. For propellant fire accident scenarios, a key property of interest is the heat transfer characteristics with respect to objects inside and adjacent to the propellant fire plume.

Although many studies have centered on measuring and modeling burn rate characteristics of propellants, less effort has been focused on characterizing the heat transfer properties from metallized propellants. The heat transfer characteristics of gas and liquid flames have been widely investigated. Calorimeters of various types (button, rod, cylinder, etc.) have been used to measure heat flux from fire plumes. Large diameter hydrocarbon pool fires have been the subject of many of these studies [16–18]. One study showed that heat fluxes generated by such fires can be up to 150 MW/m$^2$ [19].

For some gas–air flames, it has been shown that up to 90% of the heat transfer may occur by forced convection from the combustion gases to a surface [20]. Wu et al. [21] characterized the heat transfer from radial jet reattachment combustion (RJRC) using a methane–air mixture. They showed peak RJRC heat fluxes on the order of 130–190 kW/m$^2$. Kwok et al. [22] investigated the heat transfer characteristics of premixed butane–air impinging flame jets from slot and round burners. They recorded heat flux and temperature from flame impingement on a square, actively cooled impingement plate. Heat fluxes for various Reynolds numbers and air–fuel ratios ranged from 200 to 375 kW/m$^2$.

Various investigations have been made into the heat transfer enhancements of particles when added to nonreacting pipe or duct flows. Murray [23] showed that the majority of the heat transfer to a tube in gas-particle crossflow was driven by transport of thermal energy from rebounding particles. Another study isolated the effect of conduction between impacting particles in an impinging jet flow.

Received 3 October 2006; revision received 13 April 2007; accepted for publication 16 July 2007. 

*Mechanical Engineering Department.
†Materials and Metallurgical Engineering Department.
‡Engineering Sciences Center.

**Table 1 Powder properties**

| Powder composition | Mean diameter, $\mu$m | Standard deviationn $\mu$m | Density, g/cc | Melting point, °C | Supplier |
|---|---|---|---|---|---|
| Yttria stabilized zirconia (YSZ) | 24.04 | 19.46 | 5.9 | 2700 | Metallurgical Technology (Pearland, TX) |
| Alumina–13% Titania ($Al_2O_3$-$TiO_2$) | 24.55 | 12.15 | 3.9 | 1865 | St. Gobain (Northampton, MA) |
| Aluminum (Al) | 25 | 13 | 2.7 | 660 | Valimet (Stockton, CA) |

It was found that conduction was the main contributor to the enhancements of the heat transfer properties of the jet [24].

Other studies examined the addition of nonreacting particles to combustion systems. Baek et al. [25] examined the addition of 47.1 $\mu$m average diameter aluminum oxide ($Al_2O_3$) to a hydrogen–air flame to quantify the heat transfer effects of nonreacting solid particles. They showed that the presence of $Al_2O_3$ in the flame does not appreciably affect radiative heat transfer to a wall. But, by adding reactive carbon particles to the flame, they showed that both radiative and convective heat transfer values were increased over those for the flame without particles. Boron, magnesium, and aluminum are all metallic fuel additives which have been investigated for use in solid propellant formulations [26–29]. Transmission electron microscopy (TEM) techniques have been used to study size and morphology of alumina nanoparticles generated from solid rocket propellant. Karasev et al. [30] investigated the aluminum combustion stages and agglomeration using TEM analysis. With all that is known about aluminum combustion, the heat transfer characteristics of particle-laden formulations have been less commonly investigated. The heat flux investigation is much less complete than more traditional solid particle burning characteristics like ignition time and burn rate.

The environment created by an open air solid rocket propellant fire can be characterized as severe, with temperatures reaching 3000 K and heat fluxes reaching approximately 200 W/cm$^2$ [31,32]. Jackson [33] used NASA's Chemical Equilibrium Analysis (CEA) software to compare adiabatic flame temperatures and product compositions from various propellant flames and fires assuming chemical equilibrium exists during the reaction. Regarding adiabatic flame temperatures, results from [33] show good agreement between temperatures produced by various mixture ratios associated with an acetylene–oxygen flame in this study to the propellant flame and fires [31]. It is noted that the acetylene–oxygen flame is not a perfect stimulant for a typical AP propellant in that the chemical compositions are not the same (e.g., there is no chlorine in the acetylene–oxygen system). However, this flame produces similar temperatures and, by seeding the flame with particulates, similar particle loading levels for a propellant are also achieved [33]. In this way, a seeded acetylene–oxygen flame produces a similar environment (e.g., high temperatures with particles) expected in propellant fires.

This study will examine the heat flux characteristics and aluminum combustion dynamics of a simulated propellant fire using an oxygen–acetylene flame seeded with three different 25 $\mu$m average diameter powders. The sample powders were studied to compare the effect of inert yttria stabilized zirconia (YSZ), melting alumina-titania, and reacting aluminum particulates. The flame is created with a thermal spray gun, which allows for a range of oxygen–acetylene ratios to be used and provides the ability to inject and control specific flow rates of powder. A screw-type powder feeder supplies the powder at a constant rate. A button-type calorimeter is inserted into the flame by a six-axis robot. A one-dimensional heat flux calculation program uses the calorimeter's temperature data to backcalculate heat flux at the surface of the calorimeter. Various oxygen–acetylene ratios are examined to determine the influence of mixture ratio on heat flux. A two-color pyrometer (model DPV-2000, Technar, Inc., Montreal, Quebec, Canada) verifies particle temperatures so that oxygen–acetylene ratios can be adjusted to achieve similar particle temperatures for the various powders.

In addition to heat flux, the Al particle reactivity is also investigated in terms of percent Al reacted as a function of standoff distance and mixture composition. Polished copper coupons passed through the flame zone collected sample particulates. These particulates are analyzed using a scanning electron microscope with an energy dispersive spectroscopy attachment to verify the presence of aluminum oxide. Differential scanning calorimetry was also used to quantify the consumption of Al and estimate the amount reacted as a function of standoff distance. To the authors' knowledge, this is a new and innovative approach for determining the quantity of reactant that has oxidized after a specified period. The results presented provide valuable information about heat flux characteristics and general reaction dynamics for flames associated with propellant fires.

## Experimental

### Sample Powders

Table 1 shows important properties and the supplier of each powder. The powders were chosen based on their melting points, chemical reactivity, and mean particle diameter. For example, inert yttria stabilized zirconia has a high melting point and will not melt or react in the flame zone. In contrast, alumina-titania ($Al_2O_3$-$TiO_2$) will melt but will not react with the gaseous flames. Finally, Al particles will melt and react with the flames.

For experiment repeatability, it was necessary to have similar mean diameters for each of the three powders. The three different powders were examined separately. The mean and standard deviation of particle diameters were determined with a Coulter particle size analyzer. The particle densities and melting temperatures are reported from [34].

### Burner Apparatus and Calorimeter

Figure 1a is a schematic of the experimental apparatus. It depicts the four major components of the experiment: the torch, calorimeter, control arm, and data acquisition computer. A premixed oxygen and

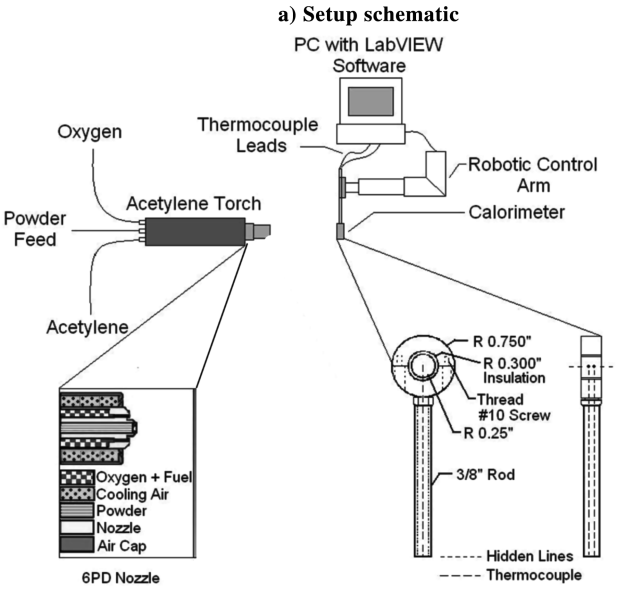


**Fig. 1 Schematic of the experimental apparatus: a) overall schematic, b) enlargement of the torch nozzle and air cap, c) enlargement of the calorimeter.**

acetylene flame was generated using a Sulzer-Metco 6P-II (Sulzer-Metco, Westbury, New York) combustion powder thermal spray gun. The torch was fitted with a type-D nozzle (Sulzer-Metco, Westbury, New York) and a gun-cooling air cap. Preliminary experiments showed that the type-D nozzle provides the hottest flame conditions, which most accurately simulates the propellant fire environment. The gun-cooling air cap uses a compressed airstream to cool the torch nozzle.

Figure 1b shows an expanded view of the nozzle and air cap used in the experiment. The nozzle cross section on the left shows each channel and its contents. The image on the right shows the distribution of cooling air from the air cap. This air serves only to cool the brass nozzle on the torch and does not participate in the combustion process. The 6P-II torch has a mixing channel that provides homogeneous blending of fuel and oxygen and a powder-feed channel that introduces the powder directly into the flame at the tip of the nozzle.

Temperature measurements from the impinging flame were made by a 304 stainless steel (SS), button-type calorimeter, instrumented with two type-K thermocouples (TCs) (Omega Engineering, Inc., Stamford, Connecticut), spaced 4.23 mm apart. Figure 1c shows a schematic of the calorimeter. The instrumented button was insulated with alumina felt and clamped in a 304 SS ring. The ring is threaded and locked onto a 0.953 cm rod. The calorimeter is attached to a mounting plate inserted into the flame by a six-axis, automated robot. The experiment is controlled by computer using LabVIEW (National Instruments, Austin, Texas) to ensure that all flow rates and robot actions are precisely executed and monitored.

#### Heat Flux Calculations

The time–temperature response of the thermocouples in the button-type calorimeter was used to calculate the surface heat flux by means of an inverse heat conduction algorithm. Temperature data were recorded from the calorimeters at 1000 Hz. The data were calculated using IHCP1D, a one-dimensional heat flux calculation program (Beck Engineering Consultants Co., Okemos, Michigan). Measurements for the gas-only flames were made to establish a baseline, and then measurements from the particle-laden flames were made. For each flow condition, a minimum of six calorimeter measurements were made to provide an average over the range of measurements and establish test repeatability.

#### Particle Collection Coupons

The particulate samples were collected on 5 $cm^2$ polished copper coupons that are fixed to the robot and passed through the flame at a rate of 63.5 cm/s. Each coupon was weighed and marked before use in the experiment. Copper was chosen as the substrate material because of its high thermal conductivity. Calculations performed using the lumped capacitance method showed that with an initial temperature of 24°C, the coupon's final temperature was approximately 33°C after passing through the flame. This small temperature change indicates that the Al particles collected on the surface are quenched such that the Al combustion reaction is halted.

#### Experimental Technique

The first set of experiments was run with gas-only flames and established baseline flame conditions. For the second set of experiments, particles were added to the oxygen–acetylene flame via a TAFA powder feeder (Concord, New Hampshire) and the powder-feeder gas flow rate was measured with a standard flow meter at the inlet to the feeder. To ensure that the particle feed was constant, individual tests were run to establish deposition consistency for the powder feeder and impingement surface. Figure 2 shows the weight of $Al_2O_3$-$TiO_2$ particles deposited on the coupon surface as a function of time in the flame and is representative of the linear trend of all particles examined. The deposition rate is linear with narrow error bars signifying good repeatability of the powder feeder. The experiments reported here were repeated for each of the powder types and conditions presented in Table 2.

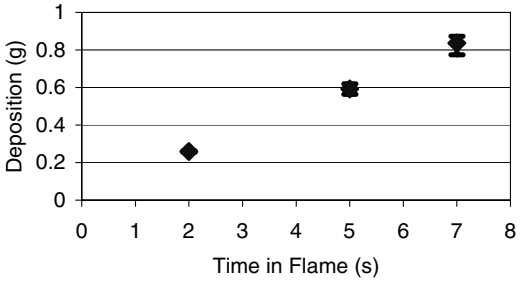


**Fig. 2 Deposition rate for $Al_2O_3$-$TiO_2$ particles collected for an oxygen–acetylene ratio of 1.5 and a total flow rate of 2.124 $m^3/h$.**

Particle temperature and velocity measurements were made using a two-color pyrometer and particle Doppler velocimeter (PDV), respectively; both measuring techniques were made using the model DPV-2000 (Technar, Inc., Montreal, Quebec, Canada). These measurements were made so that the oxygen–acetylene ratio could be adjusted to achieve uniform particle temperatures for the three powder types. The target particle temperature was specified at approximately 2100°C which is above the melting temperature of $Al_2O_3$-$TiO_2$ (Table 1). Maintaining particle temperatures of 2100°C will allow $Al_2O_3$-$TiO_2$ to melt but YSZ will remain an (inert) solid. In this way, the calorimetry measurements will reveal the effect that particle phase has on the total heat flux. The heat flux from molten and solid (inert) particles was then compared with that of reacting Al particles. This comparison serves to demonstrate and quantify the heat contribution effect of adding Al particles to the flame. The variation in oxygen–acetylene ratio associated with maintaining constant powder particle temperatures of 2100°C is directly proportional to the measured changes in heat flux indicative of inert, melting, or reacting particles. In this way, adding particles to the torch flow sacrifices a higher flame temperature (unseeded flame) for a higher effective heat transfer coefficient (particle-laden flame). Therefore, the overall heat transfer efficiency (i.e., ratio of energy delivered to a surface compared with energy available in the flow) increases with the addition of particles.

To reach the target particle temperature, the oxygen–acetylene ratio was adjusted according to the powder flow conditions. For a nozzle diameter $D$ of 4 cm and an oxygen–acetylene mixture viscosity $\mu$ of $21 \times 10^{-6}$ kg/ms [35], and a mass flow rate $\dot{m}$ equal to the mixture density 0.5690 $kg/m^3$ [35] multiplied by 2.124 (Table 2), the torch gas flow produces a Reynolds number ($Re = 4\dot{m}/\pi D\mu$) equal to 501 (i.e., laminar flow). Low powder flow rates correspond to 10.44 g/min for YSZ, 6.9 g/min for $Al_2O_3$-$TiO_2$, and 4.78 g/min for Al. The same oxygen–acetylene ratio was used for each powder such that the target particle temperature of 2100°C was achieved and the resulting heat flux measurements from the calorimeter were a clear indication of inert

**Table 2 Detailed experimental conditions**

| Powder | Oxygen- acetylene ratio | Standoff distance, cm | Torch gas flow rate, $m^3/h$ | Powder gas flow rate, $m^3/h$ | Powder feed mass flow rate, g/min |
|---|---|---|---|---|---|
| YSZ, low | 2.5 | 12.7 | 2.124 | 0.2832 | 10.44 |
| YSZ, high | 2.25 | 12.7 | 2.124 | 0.2832 | 17.41 |
| $Al_2O_3$-$TiO_2$, low | 2.5 | 12.7 | 2.124 | 0.2832 | 6.9 |
| $Al_2O_3$-$TiO_2$, high | 1.62 | 12.7 | 2.124 | 0.2832 | 11.5 |
| Al, low | 2.5 | 12.7 | 2.124 | 0.2832 | 4.78 |

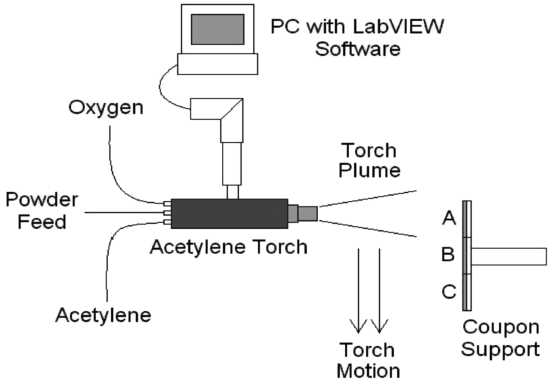


**Fig. 3 Experimental apparatus for particle collection.**

(or baseline heat flux), melting, or reacting particles. The high flows are compared with the low flows to demonstrate the effect of powder flow rate on heat flux. High powder flow rates are 17.41 g/min for YSZ and 11.5 g/min for $Al_2O_3$-$TiO_2$. No high flow rate experiments were performed for Al. An oxygen–acetylene ratio closer to stoichiometric was used for the $Al_2O_3$-$TiO_2$ so that particle temperature would be similar to that of YSZ.

Table 2 provides a summary of the parameters associated with each particle-laden flow. The "low" and "high" designation refers to the specific flow conditions used for each run and are summarized in Table 2.

When all gas line pressures were stabilized, the torch was lit manually. The robot control was initialized and the calorimeter was inserted into the gas-only flame for four separate measurements corresponding to 10 s durations. Before each measurement, the calorimeter was allowed to cool to 50°C. Numerical simulations showed that for exposure times greater than about 10 s, multidimensional heating effects become significant, which would cause the one-dimensional inverse heat transfer algorithm to give erroneous heat flux results. After this preheating process, the powder feeder was activated and began dispersing particles into the flame, and the calorimeter was inserted into the particle-laden flame. Again, after 10 s of exposure, the calorimeter was removed.

A slightly different setup was used for the Al particle collection experiments. Figure 3 depicts the setup.

This setup employed a six-axis robot to control the torch motion. The coupons were mounted side by side in an aluminum frame. The robot passed the torch over the coupons at a rate of 30.48 cm/s and particulate samples were collected on the exposed surface of the coupons.

## Results

### Heat Flux Measurements

Figure 4 shows the average heat flux results from all calorimeters for the gas-only flames. The gas-only values were used as a baseline for comparison with the particle-laden flames. The three oxygen–fuel ratio (OFR) values that were investigated were chosen because preliminary tests showed that the OFR-powder pairings seen in Table 2 were necessary to achieve consistent particle temperature in the flame zone. Figure 4 shows that as the oxygen–acetylene ratio becomes closer to the stoichiometric ratio of 1.0, the heat flux delivered by the flame increases.

Figure 5 shows a comparison between the heat fluxes from the particle-laden flames with low flow rates of each powder to that of the low-flow, gas-only flame.

Figure 6 is a summary plot of the heat fluxes for all particle-laden flames. The heat fluxes are displayed per gram mass for each powder type.

The average heat fluxes shown in Fig. 6 demonstrate the characteristics of each type of flame in the experiment. The YSZ particle flame shows the lowest heat fluxes from the group of powders. The YSZ particles are inert and the YSZ laden flames yield similar heat fluxes to the gas-only flame with the same conditions.

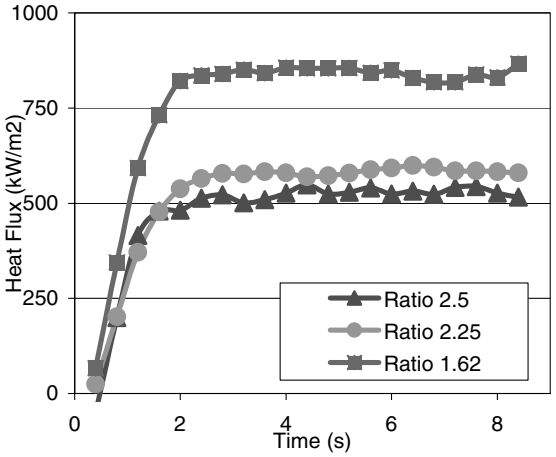


**Fig. 4 Average heat fluxes for gas-only flames.**

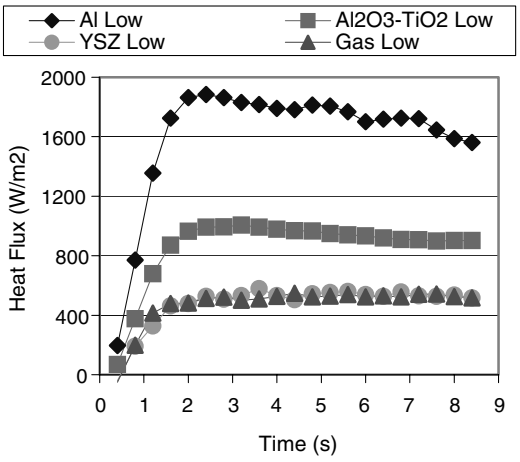


**Fig. 5 Average heat fluxes for low flow rates: gas only, YSZ, $Al_2O_3$-$TiO_2$, and Al.**

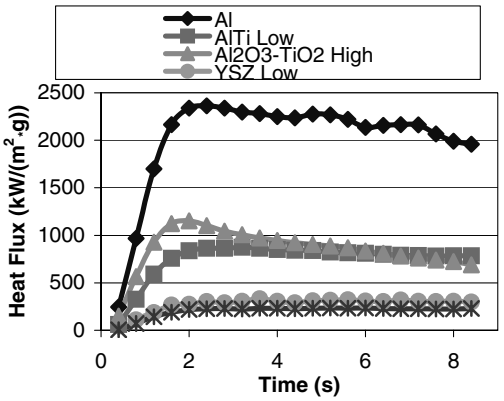


**Fig. 6 Average heat fluxes per gram powder for all particle-laden flames.**

The $Al_2O_3$-$TiO_2$ powder delivers a heat flux higher than that of the YSZ because the $Al_2O_3$-$TiO_2$ particles melt. When impinged on a cooler surface (the calorimeter), the molten particles resolidify and their latent heat provides the increased heat flux. Even higher heat fluxes are produced by the flame containing Al particles. This increase is due to the large amount of exothermic energy given off by the Al oxidation reaction.

Figure 6 demonstrates that Al provides a much greater increase in heat flux than the other powders. The heat flux values were divided

**Table 3 Comparison between IHCP1D and finite difference method**

| Location | Experimental temperature, °C | Theoretical temperature, °C | % difference |
|---|---|---|---|
| Front TC | 420.83 | 450.58 | 6.60 |
| Back TC | 238.07 | 233.46 | 1.94 |

by the total mass of each powder to which the calorimeter was exposed for each 10 s test. The heat flux per unit mass for Al is 2.7 times that of $Al_2O_3$-$TiO_2$ high flow, which provides the second highest heat flux. The Al heat flux per unit mass is 8.4 times greater than the highest heat flux per unit mass seen with the YSZ.

In Figs. 4–6, transient behaviors in the calculated heat flux are seen for times under approximately 2 s. This phenomenon is a product of the inverse method of heat flux calculation and was disregarded for all quantification of heat flux data. It is interesting to note that the heat flux for the Al and $Al_2O_3$-$TiO_2$ reaches its peak value and then drops off steadily through the rest of the run. During these tests, after a few seconds of exposure to the flame, the calorimeter became coated with Al and $Al_2O_3$-$TiO_2$ deposits. By the end of the run, there was a coating ranging from 1–5 mm in thickness on the impingement surface of the calorimeter. This coating acted as an insulator, dissipating the heat from the flame contact zone and decreasing the measured heat flux throughout the end of the run. With the low-flow of $Al_2O_3$-$TiO_2$, the same effect can be observed, but on a much smaller scale. This insulating effect is not seen with the YSZ seeded flame because the particles did not melt and therefore did not build up on the calorimeter surface.

### Heat Flux Uncertainty Analysis

A finite difference heat transfer code was employed to supplement the IHCP1D heat flux calculations. The code explicitly solves the one-dimensional heat conduction equation for the temporal derivative using a forward difference method [36,37] and the spatial derivative using a central difference method. This routine applied the IHCP1D calculated heat flux value and backcalculated the temperatures at both thermocouple locations in the button calorimeter. Table 3 is a summary of the calculated results.

The calculation shows a slightly higher difference between the theoretical and experimental temperatures for the front thermocouple location. This is expected because the front thermocouple faces a more dynamic heat flux environment, whereas the back thermocouple is more isolated from the heat flux environment by the button material. Many factors, like testing environment, thermocouple response time, thermal lag, and inherent heat transfer code assumptions and simplifications, can all contribute to this difference. Based on these calculations and the experimental diagnostics, an order of uncertainty of 7% is assigned to the experimental data.

### Scanning Electron Microscopy

The coupon weight before and after the experiment was compared to verify reliable particle collection. The collected samples were analyzed with a scanning electron microscope (SEM) using energy dispersive spectroscopy (EDS). This analysis provided information on the morphology and surface composition of the captured particles. Results showed that the most predominant element visible is Al. Other elements having a significant presence in the test area are O and Cu. It can be inferred that the oxygen is present from the $Al_2O_3$ leftover from the combustion of Al. The copper, which is seen in very small quantities, is from the coupon upon which the samples were collected.

### Differential Scanning Calorimetry

These data were coupled with thermal analysis performed using a NETZSCH (Selb/Bavaria, Germany) STA 409 PC/4/H Luxx Simultaneous TG-DSC/DTA with a temperature range from 25 to 1100°C.

The copper coupons were scraped to remove the captured particulates. Samples of approximately 4.6 mg were weighed and poured into a platinum crucible with an alumina liner. The powder samples were then hand pressed in the crucible to achieve good sample to sensor surface contact.

The calorimetry furnace was evacuated to 1.6E-4 mbar and then backfilled with standard argon (<5 ppm oxygen). Heating rates of 20°C/ min were used. A sensitivity calibration was done using a least-squares curve fit to an 8 deg polynomial from differential scanning calorimeter (DSC) data of a sapphire sample with a known specific heat. A temperature calibration was done based on the melt onset temperature of pure metal samples of indium, tin, zinc, aluminum, and gold with an applicable temperature range from 156 to 1064°C. A baseline correction was also applied to each scan based on the thermal response of an empty crucible.

Initial DSC results are presented in Fig. 7. The conditions for this sample were an oxygen–acetylene ratio of 1.5, a total flow rate of 2.124 $m^3/h$ and a standoff distance of 12.7 cm. The figure shows heat flow and temperature as a function of time for a heating rate of 20°C/ min. The heat flow curve shows a melting endotherm with an onset temperature of approximately 660°C, which corresponds with the melting temperature of Al [1]. This analysis suggests that elemental Al was present in the sample collected from the coupon and thus full oxidation of the aluminum powder did not occur. These results are consistent with the EDS element map from Fig. 8 which also indicates an abundance of Al in the collected particulate.

To gain insight into the Al combustion dynamics, the next set of experiments used the DSC to compare Al combustion using two different oxygen–acetylene ratios with various standoff distances.

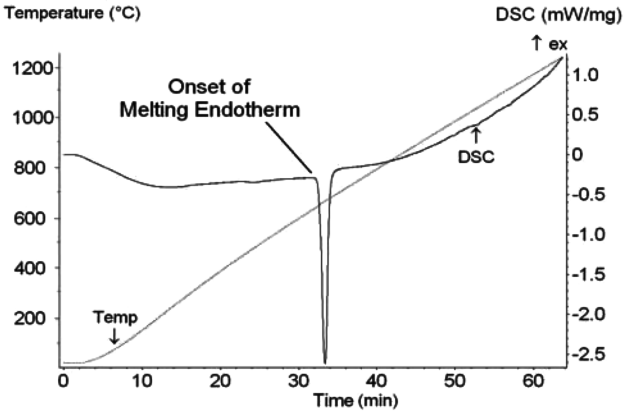


**Fig. 7 Heat flow and temperature as a function of time for a heating rate of 20°C/ min.**

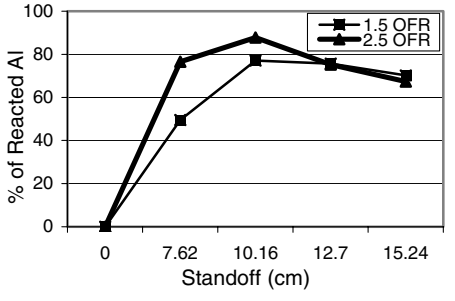


**Fig. 8 Percent of reacted Al for 1.5 and 2.5 OFRs.**

The product residue from the copper coupons was analyzed for oxygen–acetylene ratios of 1.5 and 2.5 with standoff distances of 7.62 cm, 10.16 cm, 12.7 cm, and 15.24 cm. Samples were collected from each point a minimum of three times to establish repeatability.

First, a sample set was established for unreacted Al from the supplier batch. Three thermal analysis measurements were made with the unreacted Al and the DSC area results were averaged. Each measurement quantifies heat flow as a function of temperature for heating rates of 20°C/ min. The endotherm corresponding to melting was determined and the area under each curve was calculated with a constant temperature method. The area under each curve was evaluated throughout the same temperature range to ensure consistent results. This area is directly related to the amount of elemental Al contained in the sample. The area obtained from the unreacted Al test was qualitatively deemed 100% of the available Al energy. Then the samples collected from the two oxygen–acetylene flames and four standoff distances were analyzed in the DSC. The area of each data point was averaged and the result was calculated as a percentage of Al reacted. Figure 8 shows the results for torch conditions with oxygen–acetylene ratios of 1.5 and 2.5.

Both EDS and DSC diagnostics were initially used to confirm the consumption of active aluminum in the flame. Further DSC data, coupled with the results from the heat flux portion of the experiment, were used to investigate the heat flux contribution of Al to the flame. Using the baseline Al DSC curve, a method for determining percentage of reacted Al at various points in the flame was devised.

## Discussion

### Heat Flux

Figure 5 shows that 25 $\mu$m alumina-titania ($Al_2O_3$-$TiO_2$) powder provided a 76.9% increase in average heat flux (for low flow rates) over the yttria stabilized zirconia particles of the same average diameter. One explanation for this increase in heat flux is that $Al_2O_3$-$TiO_2$ has a lower melting point than YSZ (Table 1). When injected into the flame, the $Al_2O_3$-$TiO_2$ particles were heated enough to reach their melting point, whereas the YSZ particles were only heated to a temperature close to that of the combustion gases, significantly less than the melting temperature of YSZ. When the melted $Al_2O_3$-$TiO_2$ particles impacted the calorimeter, they were quenched and released latent heat. The nonmelted YSZ particles impacted the calorimeter with a temperature similar to that of the combustion gases, hence the heat flux values for YSZ and gas-only flames were comparable. It is seen that the latent heat of a melting particle is a significant contributor to heat flux imparted to a surface. Further analysis was performed with the addition of Al particles to the flow. For low flow conditions, Fig. 5 shows that the addition of Al yielded heat flux values 84.6% higher than $Al_2O_3$-$TiO_2$ and 226.5% higher than YSZ. Figure 6 depicts the heat flux contribution of each particle on a mass basis. The average heat flux values for each powder were divided by the mass of each powder to which the calorimeters were exposed for each run. This shows that on a mass basis, Al provides heat flux enhancement 166.7% greater than $Al_2O_3$-$TiO_2$ and 613.3% greater than YSZ. This implies that the heat flux increase provided by reacting particles is mass proportional, which is expected.

### Scanning Electron Microscope/Energy Dispersive Spectroscopy Analysis

The EDS analysis verified the presence of oxygen in the collected particulates, likely present in the form of $Al_2O_3$. The elemental map and visual morphology of the collected particulates both show oxidation of Al. The intensity of Al is much greater than that of O, which suggests that there is excess Al in the collected samples. The DSC results shown in Fig. 7 confirm the results from the EDS element map. The presence of an endotherm at the melting temperature of Al indicates that some elemental Al remains in the collected sample. The heat flux measurements imply that the Al is at least partially reacted. In particular, the sharp increase in Al heat flux compared with the $Al_2O_3$-$TiO_2$ shows that the Al is releasing chemical energy. If it were simply melting, the heat flux values would be similar to that of $Al_2O_3$-$TiO_2$.

The DSC results from Fig. 7 shows that with an oxygen–acetylene ratio of 1.5 and a standoff distance of 7.62 cm, the Al oxidation had consumed approximately 54% of the available Al. At a standoff of 10.16 cm, approximately 77.1% of the available Al had been consumed. The data show unexpected results at standoff distances greater than 10.16 cm. At these distance, the Al has reached a lower percentage of reaction than for the closer standoff distances. The increase in active Al content beyond 10.16 cm is difficult to reason because it is impossible that the Al has been reacted to a lesser degree at distances farther from the torch nozzle (beyond 10.16 cm). There are many factors that could contribute to the increased Al content observed. For example, there are some intricacies of the experimental procedure that affect the selectivity of particle samples taken from large standoff distances. Each of these factors would cause an increased amount of less reacted Al particles to be collected on the copper coupon.

First, the density changes associated with oxidation of elemental Al have adverse effects on the mass of particles in the flame flow. Elemental Al has a density of 2.7 g/cc whereas $Al_2O_3$ has a density of 3.97 g/cc. It is possible that postreaction agglomerations of $Al_2O_3$ particles can weigh up to 47% more than their Al counterparts. This density change may contribute to an altered flight path of the particles, making the collection technique inherently less likely to collect the more dense, reacted $Al_2O_3$ particles. Liang [38] observed similar inertial effects during particle deposition tests. They observed that a decrease in particle size of one order of magnitude could cause up to one order of magnitude decrease in particle deposition velocity. Another factor which could cause differences in the particle collection technique is the structure of the flame produced by the structure of the oxygen–acetylene torch. At larger standoff distances, the flame zone is broader along the centerline of the torch. The flame zone from the torch has been observed to experience approximately a 50% increase in diameter at standoff distances greater than 10.16 cm. It is possible that divergence of the combustion gases and buoyancy effects could cause more particles to miss the copper coupon.

In addition to the change in property effects, other authors [39,40] have documented particle-free zones near hot walls during axisymmetric impingement experiments. These particle-free zones are a result of small diameter particles that remain in the gas flowfield around an impingement surface. These particles with less mass simply do not have enough inertia to carry them onto the impingement surface. It is unfeasible that the highly active flame zone used in the 1.5 and 2.5 OFR experiments would have a particle-free zone, but the same effect could cause a slight change in the particle collection characteristics at larger standoff distances. Jayaraj [41] investigated thermophoretic flow over inclined plates and showed that as fluid properties (density, viscosity, and thermal conductivity) increase, the wall concentration of particles decreased. This effect could be a factor in biasing the selectivity of particle collection during the copper coupon sampling. Other studies [42–44] point to increased particle sizes as one factor in decreased deposition efficiencies. This could be a contributing factor due to the increase in particle size caused by the oxide cap that forms on Al particles during the oxidation process. An increase in volume of up to 33% can be caused by conversion of Al to $Al_2O_3$.

Figure 8 shows that for an oxygen–acetylene ratio of 2.5 and a standoff of 7.62 cm, approximately 65.3% of the available Al had been consumed. For the entire range of data, the Al consumption percentages are higher than those for the oxygen–acetylene ratio of 1.5. This result is intuitive because the theoretical stoichiometric oxygen–fuel ratio for acetylene is 3.07. It would follow that a flame with an oxygen–acetylene ratio closest to the stoichiometric ratio would provide the most rapid and efficient Al oxidation because the flame provides more energy to aid in this reaction. Hence, the flame with an oxygen–acetylene ratio of 2.5 has higher reaction percentages than those for the oxygen–acetylene ratio of 1.5 for standoff distances 10.16 cm and closer.

The same irregularity that was seen with the Al reaction percentage from the 1.5 OFR flame occurs at 10.16 cm standoff with

the 2.5 OFR flame. The variation in the data is more pronounced for the 2.5 OFR flame. This is evident because there is a larger amount of $Al_2O_3$ from the Al oxidation reaction present in the 2.5 OFR flame. The larger disparity in the 2.5 OFR flame may indicate that property effects (density and size variations, thermophoretic properties, inertial effects, etc.) could be the primary cause of the data fluctuation at larger standoff distances.

## Conclusions

The heat transfer characteristics of flames seeded with various sample powders were studied to compare the effect of inert yttria stabilized zirconia (YSZ), melting alumina-titania ($Al_2O_3$-$TiO_2$), and reacting aluminum particulates. Experiments were performed with an acetylene–oxygen thermal spray gun. This apparatus was chosen because it closely simulates the temperatures and gas velocities found during the combustion of rocket propellants. Testing at low flow rates showed that flames seeded with $Al_2O_3$-$TiO_2$ provided a 76.9% increase in average heat flux over YSZ and gas-only flames. This is explained by the latent heat given off when molten $Al_2O_3$-$TiO_2$ particles solidify on the surface of the calorimeter. Aluminum-laden flames provided heat fluxes 84.6% higher than $Al_2O_3$-$TiO_2$ and 226.5% higher than YSZ. This shows that the Al particles are oxidizing in the flame and therefore releasing a large amount of chemical energy. The three particle seeded flames responded as predicted for inert, melting, and reacting particles. The consistent measurements, combined with a 7% uncertainty, verify that the experimental technique and equipment provide consistent and reliable results.

Particulate samples were collected by impingement on copper coupons and analyzed using scanning electron microscopy with an energy dispersive spectroscopy attachment. Thermal measurements of the collected Al samples were made using a differential scanning calorimeter. The EDS map showed the presence of Al and O, indicating that an oxidation reaction had occurred. The large amount of Al present indicated that the Al was not fully oxidized in the flame. Calorimetry data also showed that the Al was not fully oxidized.

Further DSC analysis was performed to isolate and compare the effects of oxygen–acetylene ratio and standoff distance on Al reaction percentages. As the oxidizer fuel ratio approaches stoichiometric, the Al consumption percentages increase. With more energy available in the gas-phase chemistry, the Al particle reactivity increases accordingly. Standoff distance was also observed to affect Al combustion percentages. The results showed that the amount of Al reacted increased with standoff distance increased up to a critical distance of 10.16 cm. Beyond this standoff distance, physical and thermal properties of particulates bias sample collection leading to misleading results.

## Acknowledgments

Technical and financial assistance for this work were provided by the Fire Science and Technology Department and the Thermal Spray Research Laboratory at Sandia National Laboratories. Sandia is a multiprogram laboratory operated by Sandia Corporation, a Lockheed Martin Company, for the U.S. Department of Energy's National Nuclear Security Administration under contract DE-AC04-94AL85000. Michelle L. Pantoya and Randy B. White would also like to acknowledge partial support for this project from the Army Research Office, contract number W911NF-04-1-0217.

## References

[1] Glassman, I., "Metal Combustion Processes," *American Rocket Society Preprint*, Periodicals Service Co., Germantown, NY, 1959, pp. 938–959.

[2] Pokhil, P. F., Belyayev, A. F., Frolov, Yu, V., Logachev, V. S., and Korotkov, A. I., "Combustion of Powdered Metals in Active Media," Nauka FTD-MT-24-551-73, 1972.

[3] Law, C. K., "A Simplified Theoretical Model for the Vapor-Phase Combustion of Metal Particles," *Combustion Science and Technology*, Vol. 7, No. 5, 1973, pp. 197–212. doi:10.1080/00102207308952359

[4] Prentice, J. L., "Combustion of Laser-Ignited Aluminum Droplets in Wet and Dry Oxidizers," *12th Aerospace Sciences Meeting*, AIAA Paper 74-146, 1974.

[5] King, M. K., "Modeling of Single Particle Aluminum Combustion in $CO_2/N_2$ Atmospheres," *17th International Symposium on Combustion*, Combustion Inst., Pittsburgh, PA, 1977, pp. 1317-1328.

[6] Kuo, K. K., *Principles of Combustion*, 2nd ed., Wiley, New York, 2005.

[7] Friedman, R., and Macek, A., "Ignition and Combustion of Aluminum Particles in Hot Ambient Gases," *Combustion and Flame*, Vol. 6, No. 1, 1962, pp. 9–19. doi:10.1016/0010-2180(62)90062-7

[8] Ermakov, V. A., Razdobreev, A. A., Skorik, A. I., Pozdeev, V. V., and Smolyakov, S. S., "Temperature of Aluminum Particles at the Time of Ignition and Combustion," *Combustion, Explosion and Shock Waves*, Vol. 18, No. 2, 1982, pp. 256–267. doi:10.1007/BF00789629

[9] Burcher, P., Yetter, A., and Dryer, F. L., "Flame Structure Measurement of Single Isolated Aluminum Particles Burning in Air," *26th International Symposium on Combustion*, Combustion Inst., Pittsburgh, PA, 1996, pp. 1899–1908.

[10] Lokenbakh, A. K., Zaporina, N. A., Knipele, A. Z., Strod, V. V., and Lepin, L. K., "Effects of Heating Conditions on the Agglomeration of Aluminum Powder in Air," *Combustion, Explosion and Shock Waves*, Vol. 21, No. 1, 1985, pp. 69–77. doi:10.1007/BF01471142

[11] Boiko, V. M., Lotov, V. V., and Papyrin, A. N., "Ignition of Gas Suspensions of Metallic Powders in Reflected Shock Waves," *Combustion, Explosion and Shock Waves*, Vol. 25, No. 2, 1989, pp. 193–200. doi:10.1007/BF00742016

[12] Rozenband, V. I., and Vaganova, N. I., "A Strength Model of Heterogeneous Ignition of Metal Particles," *Combustion and Flame*, Vol. 88, No. 1, 1992, pp. 113–118. doi:10.1016/0010-2180(92)90011-D

[13] Davis, A., "Solid Propellants: The Combustion of Particles of Metal Ingredients," *Combustion and Flame*, Vol. 7, No. 2, 1963, pp. 359–367.

[14] Melcher, J. C., Burton, R. L., and Krier, H., "Combustion of Aluminum Particles in Solid-Rocket Motor Flows," *36th JANNAF Combustion Meeting*, Chemical Propulsion Information Agency, Columbia, MD, Vol. 1, 1999, pp. 249–258.

[15] Price, E. W., "Combustion of Metallized Propellants," *Fundamentals of Solid-Propellant Combustion*, Vol. 90, Progress in Aeronautics and Astronautics, AIAA, New York, 1984, pp. 479–513.

[16] Gregory, J. J., Keltner, N. R., and Mata, R., Jr., "Thermal Measurements in Large Pool Fires," *Journal of Heat Transfer*, Vol. 111, No. 2, May 1989, pp. 446–454.

[17] Nakos, J. T., and Keltner, N. R., "Radiative-Convective Partitioning of Heat Transfer to Structures in Large Pool Fires," *American Society of Mechanical Engineers, Heat Transfer Division*, Vol. 106, No. 2, 1989, pp. 381–388.

[18] Koski, J. A., Gill, W., Gritzo, L. A., Kent, L. A., and Wix, S. D., "Characterization of Indoor and Outdoor Pool Fires with Active Calorimetry," *Proceedings of the 1995 30th National Heat Transfer Conference*, American Society of Mechanical Engineers, Heat Transfer Division, Vol. 34, No. 2, 1995, p. 79.

[19] Kramer, M. A., Greiner, M., Koski, J. A., Lopez, C., and Suo-Anttila, A., "Measurements of Heat Transfer to a Massive Cylindrical Calorimeter Engulfed in a Circular Pool Fire," *Journal of Heat Transfer*, Vol. 125, No. 1, 2003, pp. 110–119. doi:10.1115/1.1527905

[20] Viskanta, R., "Overview of Convection and Radiation in High Temperature Gas Flows," *International Journal of Engineering Science*, Vol. 36, Nos. 12–14, Sept.–Nov. 1998, pp. 1677–1699. doi:10.1016/S0020-7225(98)00053-6

[21] Wu, J., Seyed-Yagoobi, J., and Page, R. H., "Heat Transfer and Combustion Characteristics of an Array of Radial Jet Reattachment Flames," *Combustion and Flame*, Vol. 125, Nos. 1–2, 2001, pp. 955–964. doi:10.1016/S0010-2180(00)00251-0

[22] Kwok, L. C., Leung, C. W., and Cheung, C. S., "Heat Transfer Characteristics of Slot and Round Premixed Impinging Flame Jets," *Experimental Heat Transfer*, Vol. 16, No. 2, 2003, pp. 111–137. doi:10.1080/08916150303743

[23] Murray, D. B., "Local Enhancement of Heat Transfer in a Particulate Cross Flow: 1," *International Journal of Multiphase Flow*, Vol. 20, No. 3, 1994, pp. 493–504. doi:10.1016/0301-9322(94)90023-X

[24] Kurosaki, Y., Satoh, I., Kameoka, Y., and Annmo, Y., "Mechanisms of Heat Transfer Enhancement Around the Stagnation Point of an

Impinging Air Jet Laden with Solid Particles," *Proceedings of the 9th International Heat Transfer Conference*, American Society of Mechanical Engineers, Heat Transfer Division, Vol. 4, 1990, pp. 99–104.

[25] Baek, S. W., Kim, J. J., Kim, H. S., and Kang, S. H., "Effects of Addition of Solid Particles on Thermal Characteristics in Hydrogen-Air Flame," *Combustion Science and Technology*, Vol. 174, No. 8, 2002, pp. 99–116. doi:10.1080/00102200290021263

[26] Ishihara, A., and Brewster, M. Q., "Combustion Studies of Boron, Magnesium, and Aluminum Composite Propellants," *Combustion Science and Technology*, Vol. 87, Nos. 1–6, 1993, pp. 275–290. doi:10.1080/00102209208947219

[27] Chen, D. M., Hsieh, W. H., Snyder, T. S., Yang, V., Litzinger, T. A., and Kuo, K. K., "Combustion Behavior and Thermophysical Properties of Metal-Based Solid Fuels," *Journal of Propulsion and Power*, Vol. 7, No. 2, 1991, pp. 250–257.

[28] Brooks, K. P., and Beckstead, M. W., "Dynamics of Aluminum Combustion," *Journal of Propulsion and Power*, Vol. 11, No. 4, 1995, pp. 769–780.

[29] Glassman, I., and Papas, P., "Combustion Thermodynamics of Metal-Complex Oxidizer Mixtures," *Journal of Propulsion and Power*, Vol. 15, No. 6, 1999, pp. 801–805.

[30] Karasev, V. V., Onischuk, A. A., Glotov, O. G., Baklanov, A. M., Maryasov, A. G., Zarko, V. E., Panfilov, V. N., Levykin, A. I., and Sabelfeld, K. K., "Formation of Charged Aggregates of $Al_2O_3$ Nanoparticles by Combustion of Aluminum Droplets in Air," *Combustion and Flame*, Vol. 138, No. 1, 2004, pp. 40–54. doi:10.1016/j.combustflame.2004.04.001

[31] Hunter, L. W., Chang, Y., Oguz, H. N., Wilkerson, J. T., Lennon, A. M., Cain, R. P., Carkhuss, B. G., Thomas, M. E., Walts, S. C., Mitchell, C. A., Blodgett, D. W., and Terry, D. H., "Environment Created by an Open Air Solid Rocket Propellant Fire," *Combustion Science and Technology*, Vol. 179, No. 5, 2007, pp. 1003–1027. doi:10.1080/00102200600910833

[32] Widener, J. F., and Beckstead, M. W., "Aluminum Combustion Modeling in Solid Propellant Combustion Products," *Proceedings of the American Institute of Aeronautics and Astronautics*, AIAA Paper 98-3824, 1998.

[33] Jackson, M., "Development of a Propellant Simulating Gas Fueled Burner and its Applicability in the Validation of an Aluminum Particle Combustion Model," M.S. Thesis, Texas Tech Univ., May 2005 (available online at: www.etd.lib.ttu.edu/theses/available/etd-05032005-120637/unrestricted/Matt_Jackson_thesis.pdf).

[34] Weast, R. C. (ed.), *CRC Handbook of Chemistry and Physics*, 64th ed., CRC Press, Boca Raton, FL, 1984.

[35] Bailey, B. J., "Viscosity of Carbon Dioxide and Acetylene at Atmospheric Pressure," *Journal of Physics D: Applied Physics*, Vol. 3, No. 4, 1970, pp. 550–562. doi:10.1088/0022-3727/3/4/312

[36] Gerald, C. F., and Wheatley, P. O., *Applied Numerical Analysis*, 7th ed., Addison–Wesley Publishing, Reading, MA, 2004.

[37] Cengel, Y. A., *Heat Transfer: A Practical Approach*, 2nd ed., McGraw–Hill, New York, 2003.

[38] Liang, L., "Study of Effects of Inertia and Thermophoresis on Particle Deposition," Ph.D. Dissertation, Chung Yuan Christian Univ., Chung Li, Taiwan, Japan, 2003.

[39] Goren, S. L., "Thermophoresis of Aerosol Particles in the Laminar Boundary Layer on a Flat Surface," *Journal of Colloid and Interface Science*, Vol. 61, No. 1, 1977, pp. 77–85. doi:10.1016/0021-9797(77)90416-7

[40] Friedlander, S. K., Fernandez de la Mora, J., and Gokoglu, S., "Diffusive Leakage of Small Particles Across the Dust-Free Layer near a Hot Wall," *Journal of Colloid and Interface Science*, Vol. 125, No. 1, 1988, pp. 351–355. doi:10.1016/0021-9797(88)90086-0

[41] Jayaraj, S., "Effect of Brownian Diffusion and Particle Size on Thermophoretic Flow," *Proceedings of the Computers in Engineering Conference and the Engineering Database Symposium*, American Society of Mechanical Engineers, Fairfield, NJ, 1995, pp. 351–370.

[42] Derjaguin, B. V., Rabinovich, Ya. I., Storozhilova, A. I., and Shcherbina, G. I., "Measurement of the Coefficient of Thermal Slip of Gases and the Thermophoresis Velocity of Large-Size Aerosol Particles," *Journal of Colloid and Interface Science*, Vol. 57, No. 3, 1976, pp. 451–461. doi:10.1016/0021-9797(76)90224-1

[43] Talbot, L., Cheng, R. K., Schefer, R. W., and Willis, D. P., "Thermophoresis of Particles in a Heated Boundary Layer," *Journal of Fluid Mechanics*, Vol. 101, No. 4, 1980, pp. 737–758. doi:10.1017/S0022112080001905

[44] Valentin, J. R., and Smith, P. J., "Numerical Predictions of Deposition with a Particle Cloud Tracking Technique," Dept. of Chemical and Fuels Engineering Rept., Univ. of Utah, Salt Lake City, UT, 1998.

S. Son
*Associate Editor*